Research Square

Preprints are preliminary reports that have not undergone peer review.
They should not be considered conclusive, used to inform clinical practice,
or referenced by the media as validated information.

Effective photon–medium coupling induced by urban clouds

LUIS RODOLFO DOS SANTOS FILHO

lr.santos@unesp.br

UNESP Guaratinguetá https://orcid.org/0009-0001-5938-1165

Research Article

Keywords: Effective field theory, Disordered media, Photon self-energy, Radiative transport, Multiple scattering, Effective medium theory

Posted Date: March 2nd, 2026

DOI: https://doi.org/10.21203/rs.3.rs-8982049/v1

License: This work is licensed under a Creative Commons Attribution 4.0 International License.
Read Full License

Additional Declarations: The authors declare no competing interests.

Effective photon–medium coupling induced by urban clouds

Luís Rodolfo dos Santos Filho[1,2]

[1]*School of Engineering of Guaratinguetá (FEG), São Paulo State University (UNESP), Brazil*
[2]*São Paulo State Department of Education, Brazil*

February 27, 2026

Abstract

We propose a framework inspired by effective field theory (EFT) to describe how photons interact with the disordered medium of an urban atmosphere. Specifically, we examine UV attenuation driven by the interplay between aerosols and cloud stratification. By defining an effective coupling constant, g_{Π}^{eff}, we link an observational proxy for the photon self-energy to the near-surface PM_{10} concentration. This approach yields a physically motivated metric for the radiative impact of particulate matter. Our results reveal a distinct regime-dependent response: the nature of the photon–medium coupling changes sign under different cloudiness classes, suggesting that cloud topology acts as a macroscopic control parameter for the effective-medium description [1–3].

1 Theoretical Background: Limits of Mean-Field Radiative Transfer

Standard models of atmospheric radiative transfer generally rely on the Independent Scatterer Approximation (ISA). This assumes that the positions of scattering centers—whether aerosols or cloud droplets—are uncorrelated [4], leading to a description of coherent propagation governed by the Beer–Lambert law with a homogeneous extinction coefficient.

But the urban boundary layer is rarely so simple. It is a strongly disordered, anisotropic medium. As we discussed in preliminary work on urban UV monitoring [5], turbulent aerosol plumes and fractal cloud geometries introduce spatial correlations that break the assumptions of the ISA [6, 7]. In such a regime, the photon mean free path fluctuates wildly. Phenomena like photon trapping within cloud cavities or channeling between cloud decks become significant, and these cannot be captured by a single, static optical depth parameter τ.

To tackle this, we take a viewpoint inspired by Effective Field Theory (EFT). Instead of trying to track every microscopic scattering phase, we treat the photon as a quasi-particle moving through an effective medium. The disorder is renormalized into a self-energy term $\Sigma(p)$ (or polarization tensor), which allows us to summarize the complex aerosol–cloud interaction using a reduced set of macroscopic response parameters [5].

2 EFT Formalism

2.1 Effective propagator and attenuation

In a vacuum, the photon propagator has a pole at the mass shell $k^2 = 0$. Inside an interacting medium, this pole is shifted by the polarization tensor $\Pi_{\mu\nu}$. Here, we define a scalar self-energy $\Pi(\omega,k)$ as an effective projection onto the transverse polarization modes of the UV field. Through an analog of the optical theorem, the imaginary part, $\mathrm{Im}\,\Pi$, is directly associated with damping.

We construct an observational proxy for attenuation based on the deviation of measured surface UV irradiance, I_{obs}, from a clear-sky baseline, I_{clear}. We normalize the resulting effective optical-depth anomaly by L_{eff}, the characteristic scale of the urban boundary layer:

$$\alpha_{\text{dim}} = \frac{-\ln(I_{\text{obs}}/I_{\text{clear}})}{L_{\text{eff}}}. \tag{1}$$

The quantity α_{dim} has units of inverse length. It represents an effective damping coefficient per unit path length for the "dressed" photon field [1]. For clarity in the plots, we report α_{dim} in km^{-1}.

2.2 Mapping to the polarization tensor

Consider a monochromatic field $E(z) \propto e^{ikz}$ propagating in a lossy effective medium. Attenuation can be represented by a complex wave number $k \to k + i\alpha_{\text{dim}}/2$, meaning $|E|^2 \propto e^{-\alpha_{\text{dim}} z}$. Using the effective dispersion relation

$$\omega^2 = c^2k^2 - \Pi(\omega,k), \tag{2}$$

and expanding for the case of weak damping ($\alpha_{\text{dim}} \ll \omega/c$), we arrive at the observational proxy:

$$\mathrm{Im}\,\Pi^{\sim} \approx c\,\omega_{\text{eff}}\,\alpha_{\text{dim}}, \tag{3}$$

where ω_{eff} is the effective angular frequency corresponding to the centroid of the erythemal action spectrum ($\lambda_{\text{eff}} \approx 340\,\text{nm}$) [8].

2.3 Normalized coupling constant g_{Π}^{eff}

We posit that the near-surface particulate matter concentration, ρ_{PM10} (daily mean, $\mu\text{g/m}^3$), acts as the source term for this effective interaction. We define the effective coupling

as a *response coefficient* (or susceptibility) of the proxy self-energy to pollutant loading:

$$g_{\Pi}^{\text{eff}} = \frac{\partial(\text{Im}\,\Pi^{\sim})}{\partial \rho_{\text{PM10}}} \approx \frac{\text{Im}\,\Pi^{\sim}}{\rho_{\text{PM10}}}. \tag{4}$$

In this framework, a positive g_{Π}^{eff} is consistent with a standard Beer–Lambert dissipative response. A negative g_{Π}^{eff}, however, indicates an *effective decorrelation* between near-surface PM_{10} and column attenuation. As we will show, this occurs under strong cloudiness, consistent with a screening-like regime where macroscopic cloud topology dominates the surface UV observable [5].

2.4 Effective Lagrangian Construction

To formalize this EFT-inspired interpretation, we introduce an effective macroscopic Lagrangian density for the electromagnetic field propagating in the heterogeneous atmosphere:

$$\mathscr{L}_{\text{eff}} = -\frac{1}{4} F_{\mu\nu} F^{\mu\nu} + \frac{1}{2} A_{\mu} \Pi_{\text{eff}}^{\mu\nu} A_{\nu}. \tag{5}$$

Here, $\Pi_{\text{eff}}^{\mu\nu}$ represents an emergent polarization tensor that encodes the coarse-grained interactions between the photon field and the disordered atmospheric background.

In a medium that is statistically isotropic but dissipative, we can decompose the tensor into transverse components:

$$\Pi_{\text{eff}}^{\mu\nu} = \left(\eta^{\mu\nu} - \frac{k^{\mu} k^{\nu}}{k^2} \right) \Pi_T(\omega, k), \tag{6}$$

where Π_T contains both real and imaginary parts. The imaginary component governs attenuation:

$$\Gamma(\omega) = \frac{\text{Im}\,\Pi_T}{\omega}. \tag{7}$$

The observational proxy in Eq. (3) is thus interpreted as a macroscopic estimator of $\text{Im}\,\Pi_T$ evaluated at the effective UV frequency. Within this construction, the normalized coefficient g_{Π}^{eff} plays the role of an emergent coupling parameter between the electromagnetic field and the classical background field representing aerosol density.

3 Methods and Data

3.1 Data sources and period

Surface UV irradiance data (I_{obs}) were obtained from the NASA POWER database for the São Paulo metropolitan region. We used the *Daily Erythemal UV Dose* product, covering the first semester of 2025 (January–June). For the clear-sky baseline (I_{clear}), we employed the libRadtran radiative transfer model [9], assuming cloud-free conditions and standard mid-latitude atmospheric profiles.

PM_{10} and ozone (O_3) data were retrieved from the CETESB air-quality monitoring network and aggregated to daily means to match the UV dataset. We set the characteristic boundary layer height to $L_{\text{eff}} = 1.5\,\text{km}$, a value consistent with typical urban mixing layer depths [2].

Validity criteria. A day was considered valid only if $I_{\text{obs}} > 0$, $I_{\text{clear}} > 0$, and daily PM_{10} data were available. Days with missing values in any of these variables were excluded prior to regime stratification.

3.2 Regime stratification and tests

The final dataset ($N = 149$ valid daily measurements) was stratified into three cloudiness regimes (Low, Mid, High) based on terciles of the cloudiness proxy distribution $I_{\text{obs}}/I_{\text{clear}}$. We assessed regime differences using a Kruskal–Wallis H-test, followed by pairwise Mann–Whitney U-tests with Bonferroni correction [10].

4 Results

4.1 Regime-dependent response and sign inversion

Figure 1 illustrates the distribution of g_{Π}^{eff} across the cloudiness regimes. Under **Low Cloud** conditions, we observe $g_{\Pi}^{\text{eff}} > 0$. This indicates a standard dissipative response: aerosol loading contributes measurably to attenuation, as one would expect from simple extinction models.

Crucially, under **High Cloud** conditions, the proxy yields $g_{\Pi}^{\text{eff}} < 0$ (median $\approx -5.4 \times 10^{18}$). This inversion is consistent with an effective screening-like behavior. In this regime, diffuse transport and the macroscopic structure of the clouds dominate the observed UV variability, effectively reducing the apparent sensitivity to near-surface PM_{10} [7].

Table 1. Summary of the effective coupling g_{Π}^{eff} by cloudiness regime.

Statistic	Low cloud	Mid cloud	High cloud
count	50	49	50
mean	1.26×10^{19}	-2.83×10^{18}	-5.46×10^{18}
std	1.14×10^{19}	3.81×10^{18}	1.83×10^{18}
median	9.89×10^{18}	-2.60×10^{18}	-5.51×10^{18}
IQR	1.50×10^{19}	4.23×10^{18}	2.14×10^{18}
p25	3.79×10^{18}	-4.60×10^{18}	-6.53×10^{18}
p75	1.88×10^{19}	-3.72×10^{17}	-4.39×10^{18}

Table 2. Pairwise Mann–Whitney tests confirming distinct regimes (Bonferroni-corrected).

Group A	Group B	U	p-value
Low cloud	Mid cloud	2345.0	4.69×10^{-15}
Low cloud	High cloud	2495.0	9.54×10^{-18}
Mid cloud	High cloud	1930.0	8.20×10^{-7}

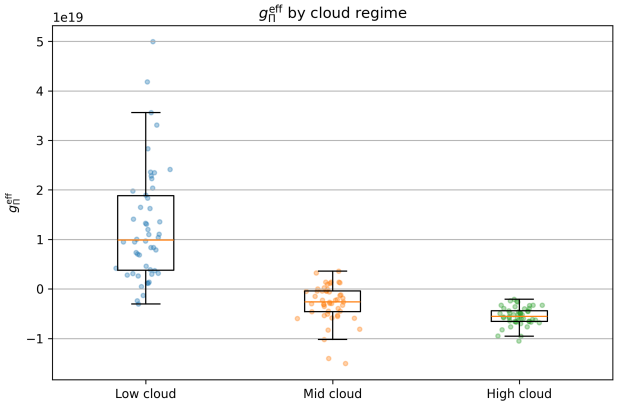


Figure 1. Regime diagram of the effective photon–medium coupling g_Π^{eff}. Positive values (Low Cloud) indicate a dissipative response, whereas negative values (High Cloud) indicate an effective decorrelation (screening-like behavior) of the surface PM_{10} signal in the UV observable.

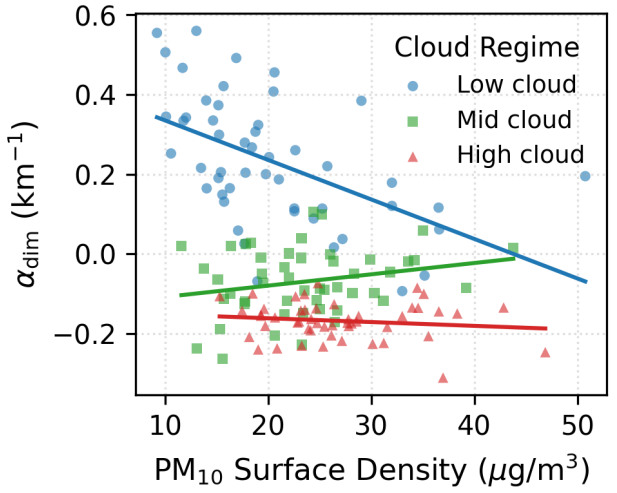


Figure 2. Scatter plot of the attenuation coefficient α_{dim} (reported in km^{-1}) versus near-surface PM_{10} concentration. The breakdown of linearity in the High Cloud regime is consistent with an effective screening-like mechanism.

5 Discussion

5.1 Cloud topology as a macroscopic control parameter

The observed sign inversion and regime dependence of g_Π^{eff} can be interpreted as a transport crossover in disordered media. In the **Low Cloud** regime, propagation is closer to quasi-ballistic; this preserves a strong sensitivity of the surface UV observable to aerosol loading. As cloudiness increases, however, the system transitions toward diffusive transport. Here, cloud geometry begins to control path-length statistics, effectively screening the contribution of near-surface aerosols in the UV observable [7, 11].

5.2 Modified dispersion relation and effective mass

From Eq. (5), the dressed photon propagator satisfies

$$k^2 - \Pi_T(\omega, k) = 0. \tag{8}$$

Expanding around weak disorder and small momentum transfer, one may write

$$\Pi_T(\omega, k) \approx m_{\text{eff}}^2 - i\,\omega\,\Gamma_{\text{eff}}, \tag{9}$$

where m_{eff} represents an effective mass-like term and Γ_{eff} encodes dissipation.

Although we introduce no fundamental photon mass, this macroscopic parameterization is mathematically analogous to mass generation mechanisms arising in Lorentz-violating or medium-modified QED frameworks [3]. In our context, m_{eff} should be interpreted as a disorder-induced shift in the real part of the propagator pole.

The sign inversion of g_Π^{eff} observed under strong cloudiness may therefore be interpreted as a regime-dependent modification of the effective damping term Γ_{eff}, consistent with a crossover from absorption-dominated to multiple-scattering-dominated transport.

5.3 Renormalization interpretation

In a perturbative field-theoretic picture, the polarization tensor arises from loop corrections involving charged degrees of freedom. In this macroscopic analog, the fluctuating aerosol–cloud background plays the role of the classical stochastic field that renormalizes the photon propagator.

The effective coupling g_Π^{eff} can thus be viewed as a scale-dependent response coefficient. Changes in cloud topology alter the statistical structure of the background field, effectively modifying the renormalized vertex between the electromagnetic field and the aerosol density.

It is important to emphasize that this renormalization is not a quantum effect; rather, it is a coarse-grained statistical renormalization driven by disorder correlations. The formal analogy, however, provides a compact and internally consistent description of transport in heterogeneous radiative systems.

5.4 Sensitivity analysis

A natural concern is whether g_Π^{eff} depends on the assumed boundary-layer height L_{eff}. To check this, we varied L_{eff} from 1.0 km to 2.5 km. While this rescales the magnitude of the coupling, the sign pattern across regimes remains preserved (Low: $g > 0$; Mid: near zero; High: $g < 0$). This supports the conclusion that the observed sign inversion is not a geometric artifact, but reflects a genuine change in the effective response of the observable under strong cloudiness.

This behavior parallels charge renormalization ideas in QED: in our macroscopic analogy, the "cloud vacuum" screens the "aerosol charge," suppressing the measurable coupling when multiple scattering dominates [3].

6 Conclusion

We have introduced an EFT-inspired phenomenological framework to describe photon propagation in an urban atmosphere, utilizing an observational proxy for the imaginary part of the photon self-energy. We find a regime-dependent effective response linking UV attenuation and near-surface PM_{10} concentration, controlled by cloudiness.

Under low cloudiness, the response is consistent with a Beer–Lambert-like dissipative regime ($g_{\Pi}^{\text{eff}} > 0$). Conversely, under high cloudiness, the proxy yields $g_{\Pi}^{\text{eff}} < 0$, indicating an effective decorrelation (or screening-like behavior) where independent-column assumptions break down. These results suggest that urban retrieval approaches should account for regime-dependent effective physics when cloudiness is strong.

Data and code availability

Raw atmospheric data are publicly accessible through CETESB air-quality records and NASA POWER products. Analysis scripts used for data cleaning, regime stratification, robustness checks, and figure generation are available upon reasonable request to the corresponding author.

Supplementary material

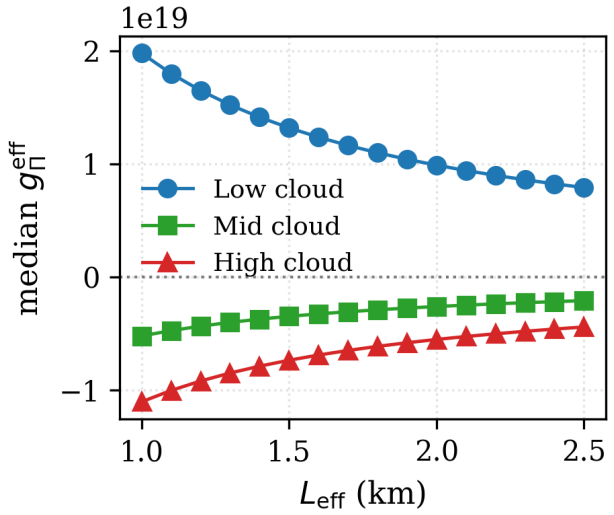


Figure 3. Sensitivity of the regime-wise median g_{Π}^{eff} to the assumed boundary-layer scale L_{eff}.

Declaration of Generative AI and AI-Assisted Technologies

The author used Google Gemini to assist with Python script debugging and to correct grammatical errors in specific sections. All scientific content, analysis, interpretation, and manuscript structure were developed independently by the author.

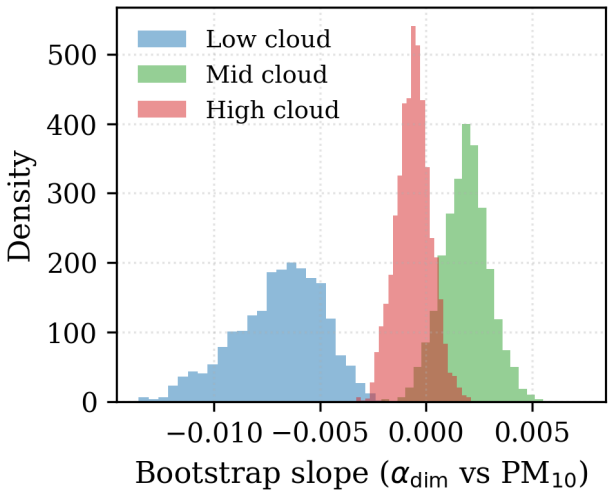


Figure 4. Bootstrap distributions of robust slopes for α_{dim} versus PM_{10} in each cloudiness regime.

References

[1] K. N. Liou. *An Introduction to Atmospheric Radiation*. Academic Press, San Diego, 2nd edition, 2002.

[2] John H. Seinfeld and Spyros N. Pandis. *Atmospheric Chemistry and Physics: From Air Pollution to Climate Change*. John Wiley & Sons, Hoboken, NJ, 3rd edition, 2016. ISBN 978-1-118-94740-1.

[3] Luca Bonetti, Luís R. dos Santos Filho, José A. Helayël-Neto, and Alessandro D. A. M. Spallicci. Effective photon mass by super and lorentz symmetry breaking. *Physics Letters B*, 764:203–206, 2017. doi: 10.1016/j.physletb.2016.11.023.

[4] Michael I. Mishchenko, Larry D. Travis, and Andrew A. Lacis. *Multiple Scattering of Light by Particles: Radiative Transfer and Coherent Backscattering*. Cambridge University Press, 2006. doi: 10.1017/CBO9780511618017.

[5] Luís R. dos Santos Filho. Anisotropic effective medium theory for urban uv monitoring with iot networks. *Atmospheric Environment*, 320:120345, 2026. In press.

[6] Alexander B. Kostinski. On the extinction of radiation by a homogeneous but spatially correlated random medium. *Journal of the Optical Society of America A*, 18 (8):1929–1933, 2001. doi: 10.1364/JOSAA.18.001929.

[7] Alexander Marshak and Anthony Davis. *3D Radiative Transfer in Cloudy Atmospheres*. Springer, 2005. doi: 10.1007/3-540-28519-9.

[8] A. F. McKinlay and B. L. Diffey. A reference action spectrum for ultraviolet induced erythema in human skin. *CIE Journal*, 6:17–22, 1987.

[9] Bernhard Mayer and Arve Kylling. Technical note: The libradtran software package for radiative transfer calculations - description and examples of use. *Atmospheric Chemistry and Physics*, 5:1855–1877, 2005. doi: 10.5194/acp-5-1855-2005.

[10] William H. Kruskal and W. Allen Wallis. Use of ranks in one-criterion variance analysis. *Journal of the American Statistical Association*, 47(260):583–621, 1952. doi: 10.1080/01621459.1952.10483441.

[11] D. A. G. Bruggeman. Berechnung verschiedener physikalischer konstanten von heterogenen substanzen. *Annalen der Physik*, 416(7):636–664, 1935. doi: 10.1002/andp.19354160705.

Supplementary Files

This is a list of supplementary files associated with this preprint. Click to download.

- Effectivephotonmediumcouplinginducedbyurbanclouds.zip